A scattering spectrometer for white light interferometry

Sun, Qi; Williamson, James; Vettenburg, Tom; Phillips, David B.; Martin, Haydn; Brambilla, Gilberto

Published in:
Optics and Lasers in Engineering

DOI:
10.1016/j.optlaseng.2023.107743

Publication date:
2023

Optics and Lasers in Engineering 169 (2023) 107743

Contents lists available at ScienceDirect

Optics and Lasers in Engineering

journal homepage: www.elsevier.com/locate/optlaseng

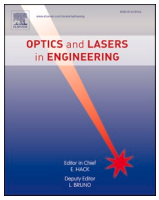

A scattering spectrometer for white light interferometry

Qi Sun [a], James Williamson [b], Tom Vettenburg [c], David B. Phillips [d], Haydn Martin [b], Gilberto Brambilla [a], Xiangqian Jiang [b], Martynas Beresna [*,a]

[a] Optoelectronics Research Centre, University of Southampton, Southampton, SO17 1BJ, United Kingdom
[b] Centre for Precision Technologies, University of Huddersfield, Huddersfield, HD1 3DH, United Kingdom
[c] University of Dundee, Dundee, DD1 4HN, United Kingdom
[d] University of Exeter, Exeter, EX4 4QL, United Kingdom

ARTICLE INFO

Keywords:
Optical scattering
Femtosecond laser processing
Interferometry

ABSTRACT

White light interferometry is a non-contact method to measure surface topography. The depth profile of the surface is typically encoded in the spectrum of the reflected light, and a spectrometer is used to decode this signal. In this work, we demonstrate a new form of spectral interferometry, a subset of white light interferometry, in which the conventional spectrometer is replaced with an engineered scattering chip and a camera. The chip is created using laser direct writing to controllably embed scattering centres within a bulk silica substrate, forming a highly stable optical scattering element. Calibration of our device is straight-forward: we circumvent the need for spectral characterisation and computational extraction of the spectrum, and instead directly measure the relationship between surface depth and the white light speckle pattern. Using our technique, we demonstrate surface profile measurements with a resolution of 27 nm over a range of 0.5 mm. Our work provides a new route to the development of potentially compact and low-cost white light interferometers with implications for the measurement of distance, strain, temperature, pressure, and more.

1. Introduction

Spectrometers yield measurements of the intensity of incident light as a function of frequency. Accurate spectral discrimination is fundamental to a wide range of technologies. Applications for spectrometers are widespread and include bio-molecular and chemical fingerprinting, materials analysis, terrestrial and astronomical remote sensing. In these examples, the data analysis typically follows a two step process: first the optical spectrum is measured using a spectrometer, and next the spectrum is converted, via a model or additional calibration step, into the information of interest such as the chemical composition of a sample, or the level of cloud cover over an ocean.

Conventional grating-based spectrometers achieve spectral discrimination by angular dispersion of light using a combination of gratings and mirrors. Depending on the precise configuration, one or more these optical elements will be curved to provide for focussing or collimation. For instance, the common Czerny-Turner configuration makes use of two curved mirrors and a planar grating. In other configurations a reduction in optical element count is achieved through the use of a curved grating. Nonetheless, conventional spectrometers often represent a major contribution to overall cost of an optical system due to need to manufacture, assemble and align these elements. Furthermore, achieving high spectral resolution requires a long optical path length by which to amplify angular dispersion, imposing a minimum limit on the size of a conventional spectrometer. While this can be alleviated to a limited degree though the use of a folded layout, the bulky nature of conventional spectrometers limit their suitability in hand-held devices and applications requiring miniaturisation and/or integration of sensors. Scattering spectrometers overcome the fundamental limitations of conventional spectrometers by relying on multiple scattering to increase the optical path in a small volume. Such devices have been proposed as a simpler, cheaper and more compact alternative to the often bulky, multi-component spectrometers. The random scattering can be realized through various means, including a multimode fibre [1], alumina (Al_2O_3) powder [2], or silicon-on-insulator scattering medium [3]. In addition, analysis of the information encoded within speckle patterns has been employed in optical time domain reflectometry from single mode fibers [4] and integrating spheres [5]. While scattering spectrometers have low component count, compact construction and outstanding sensitivity, this comes at the cost of a poor long-term

* Corresponding author.
E-mail address: M.Beresna@soton.ac.uk (M. Beresna).

https://doi.org/10.1016/j.optlaseng.2023.107743
Received 29 March 2023; Received in revised form 15 June 2023; Accepted 11 July 2023
Available online 21 July 2023

stability. Recently, direct laser writing of a pseudo-random pattern in a single solid optical chip has efficiently addressed this issue [6]. Engineering the random pattern also enables tuning of the scattering length and thus sensitivity. As for traditional spectrometers, a scattering spectrometer requires calibration, whereby speckle patterns of known spectra are acquired. Afterwards, the spectrum can be reconstructed from the observed speckle pattern by decomposing it into a weighted sum of the pre-measured individual speckle patterns generated at the calibration frequencies.

In this work we demonstrate the use of an artificially engineered scattering chip in place of a conventional spectrometer, as part of a spectral interferometry (SI) system. Spectral interferometry uses a broadband light source and spectrometer and can be considered as a sub-type of white light interferometry (WLI). SI is widely used for measurement of surface topography, distance [7–9], strain [10,11], refractive index [12,13], temperature or pressure [12]. We demonstrate the implementation of SI using a scattering chip for the measurement of surface topography. This application area is highly relevant, because within advanced manufacturing sensor cost and size are both critical issues for economic viability and the ability to integrate sensors for in-situ measurement.

The scattering chip is created using direct laser writing to embed scattering centres within the bulk of a silica substrate, forming a highly stable element in which the level of scattering, and thus the resolution of the interferometer, can be precisely engineered. Scattering based techniques have been used to demonstrate exceedingly high spectral resolution wavemeters [14,15], which track the fluctuations in the frequency of light known to consist of a single spectral component with a narrow line-width. In case of SI, the position is encoded in spectral modulation due to interference (Fig. 1b). Such spectral pattern presents a challenge for reconstruction using conventional approach as scattering spectrometers typically suffers from low signal-to-noise ratio (SNR) due to the overlap of individual wavelength caused scattering speckle. We overcome this issue by consolidating the conventional two-step data analysis into a single calibration step. Instead of first extracting a low SNR optical spectrum from the scattering spectrometer and subsequently mapping it to surface depth, here we never recover the optical spectrum and instead directly calibrate the relationship between the surface depth and the white light speckle pattern, which preserves a high SNR throughout the data processing pipeline. Compared to a traditional spectrometer, scattering chip based SI has a wider scanning range with controllable resolution. Also, it has the potential to achieve compact and low-cost solutions that foster wide-spread use of interferometric measurement systems.

2. Methodology

2.1. Scattering chip manufacture

The laser writing system was based on a PHAROS femtosecond laser (Light Conversion Ltd., Lithuania) operating at $\lambda = 1030$ nm wavelength, with a pulse duration of 200 fs and a repetition rate of 200 kHz. The laser inscription was performed with a second harmonic 515 nm beam, where the oil-immersion lens (NA 1.25) is optimized for transmission and provides aberration free focusing. Fused silica (UVFS C7980 0F) was chosen for the substrate of the scattering chip due to ultra-low thermal expansion coefficient (0.57×10^{-6} K^{-1}) and chemical inertness.

The scattering chip consists of a 20 layer random structure with an average individual scatterer spacing of 2 μm and a randomized offset of 600 nm (Fig. 1a). The distance between layers is fixed at 5 μm. The scattering medium is written 20 μm below the sample surface encapsulating the chip with pure silica. Each individual scatterer is a nanovoid formed by a microexplosion induced by a single 220 nJ femtosecond pulse, which achieves a refractive index contrast up to 0.45 [16]. To speed up the writing process, each layer of the scattering chip only has single-axis randomization. For a 1 mm × 1 mm scattering matrix, a single layer was written in 150 s, thus 50 min for a 20-layer chip.

For practical applications, it is very important to evaluate the stability of the scattering chip. By embedding the scattering layers into the silica glass substrate we achieve an effective encapsulation of the structure protecting it from the environment. As a result, any changes in the speckle patterns could only be due to a temperature variation. The temperature has a dual effect on the scattering medium: refractive index change and thermal expansion. For silica the refractive index change with temperature (dn/dT) is around $10^{-5}K^{-1}$. In previous work we have conducted a 7-day stability test with a similar scattering chip, and shown that the reconstructed wavelength can stay stable within 0.05 nm [17].

2.2. Scattering chip interferometer experimental setup

The spectral interferometer comprises three main parts, all linked with a single-mode fibre (Nufern 780HP); the light source, a remote probe and the scattering chip detection assembly. In this implementation (Fig. 2b and c) we use a Michelson probe for surface topography measurement, constructed from off-the-shelf cage system components. This may be replaced by any miniature interferometric probe optimised for distance, topography, strain, temperature or pressure measurement as necessary. The schematic in Fig. 2 shows the optical setup for calibration and performance evaluation of the scattering chip spectrometer. Light from a broadband (λ_c=850 nm, $\delta\lambda$=50 nm or λ_c=830 nm, $\delta\lambda$=25 nm) superluminescent diode (SLED) is coupled into a single-mode fibre before being split by a 50:50 fibre optic coupler (FOC1). The light from

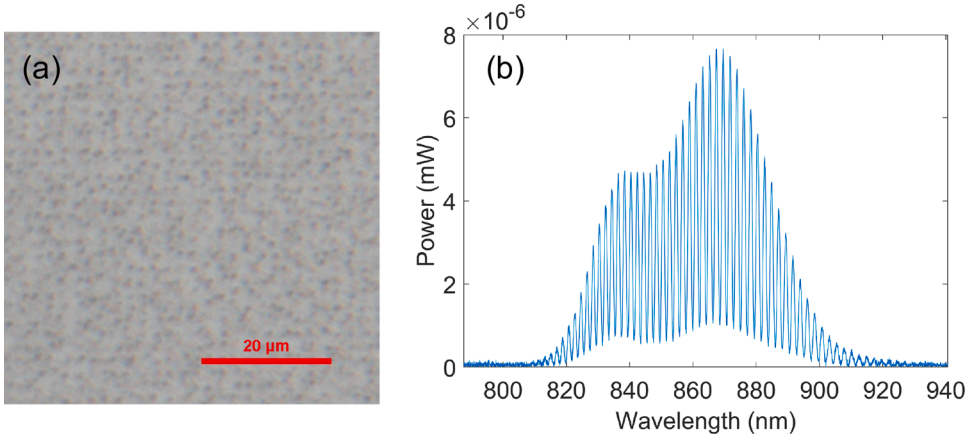

Fig. 1. (a) Close-up image of a section of the fabricated scattering chip, with individual scatterers clearly visible. (b) A typical spectral interferogram, as obtained from the apparatus shown in Fig. 2 using an optical spectrum analyser (OSA). Within the envelope of the acquired spectrum is a sinusoidal oscillation. The frequency of this oscillation is dependent on the optical path difference (OPD) in the interferometer which is in turn, directly related to the position of the measurand. The underlying mechanism for the signal generation is described by Eqs. (1) & (2).

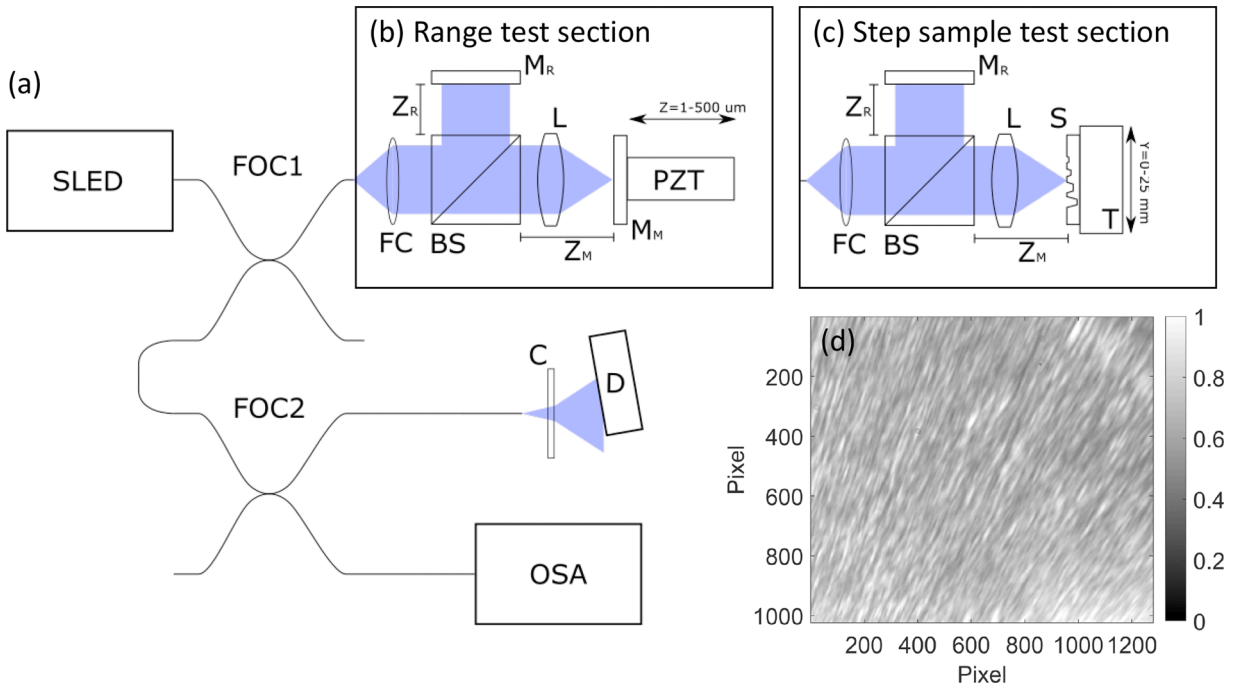

Fig. 2. (a) Schematic of the optical layout for the scattering chip interferometer, in which (b) is the section for range test and (c) is the section for step sample test. SLED is the superluminescent diode, FOC1 and FOC2 are 50:50 fibre optic couplers, FC is a GRIN fibre collimator, BS is a beam splitter, L is a doublet lens, M_M is the calibration mirror, M_R is the reference mirror, PZT is a piezo-electric translator, C is the scattering chip, D is a CMOS detector and OSA is an optical spectrum analyzer. (d) Typical speckle image for a single wavelength laser input captured by CMOS.

one arm of FOC1 arrives at the Michelson probe and is coupled into free-space by a GRIN fibre collimator (FC) before being split into the reference and measurement arms of the probe by a beam splitter (BS). In the probe reference arm light is reflected from the reference mirror, M_R, with the phase advancing by an amount $2kZ_R$. For range test setup (Fig. 2b), in the measurement arm, a doublet lens (L) focuses the measurement beam onto the calibration mirror (M_M) mounted upon a piezo-electric translator (PZT) before it passes back through to recombine with the reference beam at the beam splitter with the phase in the measurement arm having advanced by $2k(Z_M + d)$ where d is the change in measurement path length incurred by changing the PZT position. For the step sample test (Fig. 2c), the PZT has been replaced by a stepper motor translation stage (T) and the step sample (S). Following recombination of the two beams at the beamsplitter the light is recoupled back into the fibre.

The recoupled measurement and reference beams next travel through a common-mode path back through FOC1 before being split by FOC2. One arm of the coupler leads to an optical spectrum analyser (OSA) (Thorlabs OSA201C) which is included as a tool for alignment of the probe and to provide spectral interferograms for comparison; an example of such a sinusoidally shaped spectral interferogram is shown in Fig. 1b. Light exiting the second arm of FOC2 is incident upon the glass slide housing the speckle chip. A CMOS camera (D) (Pixel Link D721MU-T) captures the scattered light and speckle patterns are saved to the computer for post-processing.

The wavenumber (k) dependent phase of light arriving at the OSA is thus:

$$\theta(k) = 2kZ_R - 2k(Z_M + d) \tag{1}$$

Where d is the change in length of the measurement arm due to movement of the PZT or a measurement sample and, Z_M and Z_R are the measurement and reference arm path lengths respectively. The resulting spectral interferogram observed at the OSA can thus be described as follows:

$$I(k) = B\{k\} + A\{k\}cos(\theta\{k\}) \tag{2}$$

where $B\{k\}$ is the contribution of non-interfering DC light and $A\{k\}$ is the power spectral density of the light source, in this case a double-Gaussian. An example spectral interferogram from the OSA is shown in Fig. 1b while a speckle pattern from the scattering chip is shown in Fig. 2d.

2.3. Position mapping algorithm

The spectrum produced by the spectral interferometer high frequency modulation across whole specral bandwidth of the source (Fig. 1b). Recovering spectrum with such complex structure is challenging for scattering spectrometers due to computational errors occurring during SVD decomposition and subsequent Fourier transform for extracting position value contributing to low SNR. In addition, this approach would require a tunable light source with matching spectral characteristics for calibration. However, it is possible to utilise similar algorithm and avoid low SNR by matching speckles directly to position [6]. In this case, instead of trying to decompose a speckle pattern into multiple spectral components, we have direct match of speckle pattern to unique position of the PZT.

To calibrate the scattering chip spectrometer, the PZT is translated stepwise in the z direction (see Fig. 2b). For each PZT position, a related speckle pattern is captured by the CMOS camera. This results in a calibration intensity matrix group C(x,y,p), where p is the calibrated positions. Then for an unknown surface height, we capture a speckle pattern, M(x,y). We can then calculate the weighted correlation S(p) [6]:

$$S = C^{-1}M \tag{3}$$

The inverse of C, C^{-1}, could be calculated by directly inverting the single value decomposition $C = U\Sigma V^{\dagger}$, as

$$C^{-1} = V\Sigma^{-1}U^{\dagger} \tag{4}$$

Here, U and V are unitary matrices where the reciprocal value, †, denotes the complex transpose, Σ is a diagonal matrix with the singular values,

σ_i, of C, and Σ^{-1} is a diagonal matrix with reciprocal values, $1/\sigma_i$. Each singular value thus represents an independent link between the positions and their effects on the measured speckle pattern. The link's contribution is proportional to the singular value. From Eqs. (3) and (4), we can then get the weighted term S which converts the speckle pattern to the position information in the calibration group. However, in practice the matrix C may not be ill-conditioned and division by near-zero values σ_i would amplify the measurement error ϵ. Instead of a simple inversion, we use a Wiener filter to regularize the inversion, $\widehat{\Sigma}_i^{-1} = \sigma_i(\sigma_i^2 + |n/s|^2)^{-1}$. The term n/s is the noise over signal ratio which is set to 0.01 corresponding to a 20 dB signal-to-noise ratio (SNR) in our system. It can be noted that the inversion of singular values below the SNR are suppressed while large values are unaffected. The number of singular values above the SNR defines the number of positions the scattering chip can reliably distinguish.

2.4. Profile measurement setup

In the experiment, the calibration group is captured by reflection from a mirror mounted on a PIHERA P-625 closed-loop piezo-electric transducer (PZT) stage (Physik Instrumente, Germany) (Fig. 2b). The PZT is translated in the z direction in increments of 0.5 μm across a 500 μm range. In order to perform a profile measurement and demonstrate the suitability of the scattering chip spectrometer for white light interferometry, the PZT and measurement mirror used for calibration are replaced by a stepper motor translation stage (T) (Fig. 2c). This stage (Newport MFA-CC) has a resolution of 0.1 μm and a range of 25 mm. By mounting a measurement sample upon the stage the focal spot of the probe can be scanned across the sample to build a 2D profile measurement. Figure 2c shows the addition of the translation stage (T) and the measurement sample (S) which in this case is a reference step sample (Rubert 513).

3. Results and discussion

3.1. Range, linearity and resolution

The range of the SI setup was evaluated following calibration of the scattering chip spectrometer by translation of the measurement mirror using the PZT to move from z=0 μm to 500 μm in 0.5 μm increments with a speckle pattern captured for each increment. A second set of data, to be used as measurement data, with an increment of 1 μm is then obtained and the calibration set is used to determine the z-position of each pattern. The plot in Fig. 3c shows the result of position reconstruction results of 500 test speckle images. The x-axis shows the position information in the calibration group, the blue point shows the reconstructed position by the algorithm. Over the range of 500 μm, the reconstructed position has the std. error of ≈ 2.9 μm. Notice the step size of the PZT is 1 μm, the resolution could be further improved with finer PZT calibration steps.

We also found that the measurable range is dependant upon the coherence length of source. The result in Fig. 3c is measured with a SLED with 25 nm bandwidth and centered at 830 nm. For a 850 nm SLED with 50 nm bandwidth (Fig. 3d), we obtained a measurable range over 340 μm. Beyond 340 μm the signal strength decreases and noise increases reducing our ability to determine the surface position.

For a broadband source, due the overlap of the scattering speckle from individual wavelength, a wider bandwidth gives more random and lower SNR speckle. Figure 3a and b compare the modified speckle patterns (after background removal process) at 200 μm for 830 nm narrow bandwidth source and 850 nm wider bandwidth source. In Fig. 3a, we

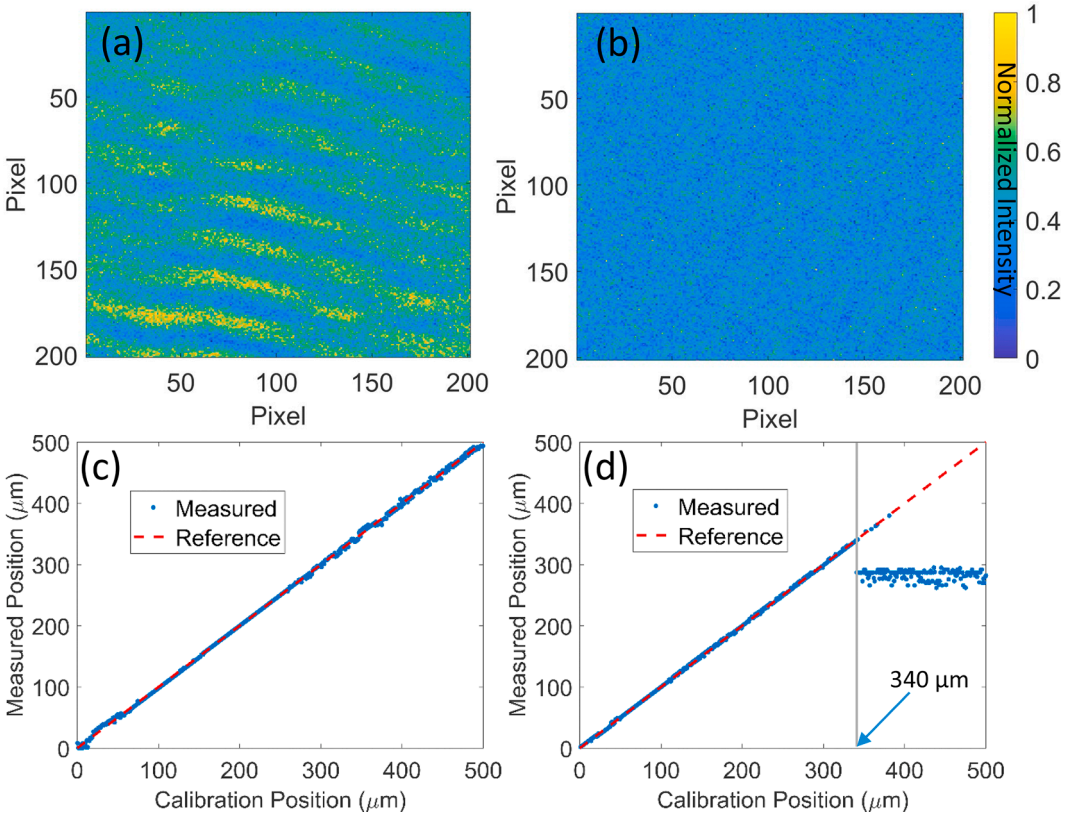

Fig. 3. Speckle patterns at 200 μm with (a) 830 nm source with 25 nm bandwidth and (b) 850 nm SLED source with 50 nm bandwidth together with position reconstruction test over 500 μm range using (c) 830 nm SLED source and (d) 850 nm SLED source. The blue marker shows the reconstructed position with each captured speckle pattern in the test group. The red line shows the actual motor position. Notice the images in (a) and (b) are cropped from 1024 × 1280 full pixel speckle pattern. (For interpretation of the references to colour in this figure legend, the reader is referred to the web version of this article.)

can see the strong interference fringes which enable the algorithm to recognize and link to the position information. However, Fig. 3b seems more random. Also, from the colorbar we can see the dynamic range of Fig. 3a is larger than Fig. 3b.

The resolution of the scattering chip spectrometer was evaluated by reducing the calibration step increment to the minimum step size of the PZT, 5 nm. Due to the time required for this high resolution calibration process was limited to a taking a sequence of 200 x 5 nm steps across a total PZT stage displacement of 1 μm. Once the calibration run was completed, the system was switched to the measurement mode. Here the stage run was repeated, with the system reporting back on the detected positions. Figure 4a shows the positions reported by the apparatus as the stage repeated the 200 x 5 nm step run; some quantisation of the measured positions is clearly evident over an 25 nm stage translation interval. An estimation of the axial measurement resolution of the system was determined to be 27 nm, obtained by applying a least-squares linear fit to the dataset and substracting the resulting gradient from the raw data before calculating the standard deviation of all data points.

At present the resolution of the method is limited by the positional accuracy and noise of the PZT control loop. The PI Hera PZT used for calibration has a resolution of 1.5 nm however the range of 500 μm reduces the stiffness of the assembly and hence has an accuracy of around 20 nm. A shorter range, stiffer PZT would allow calibration to a higher resolution though increasing the calibration steps will have penalties for the overall calibration time required.

3.2. 2D Profile measurement

Following investigation of range, linearity and resolution of the scattering chip SI setup, the PZT z-axis translation stage was replaced by a linear stepper motor. This configuration allows lateral translation of a measurement sample in the *x*-axis direction to record a 2D profile measurement.

A Rubert step height sample (Rubert 513), with steps of 30, 200, 500 and 1000 μm, was placed in front of the Michelson probe and the pitch/yaw of the sample adjusted to maximise returned light power into the fibre. A 4 mm lateral scan of the 30 μm step was performed with a speckle pattern captured at translation stage intervals of 0.01 mm resulting in 400 measured speckle patterns.

Next the captured measurement data set was post-processed in MATLAB using a 200 μm range calibration set of speckle patterns, resulting in the 2D profile measurement of step height. Profile errors resulting from reduced signal on the high slope leading into the step height were rejected based on their match to the background signal. The profile was then exported to MountainsMap (Digital Surf) software to apply automatic least squares fit levelling. Step height calculation was achieved using automatic region selection and the method described in BS ISO 5436 section A1. Fig. 4b shows the levelled step height measurement in blue and highlights the regions used by MountainsMap to calculate the step height in red. The mean depth and maximum depth of the step height measurement were calculated as 29.45 μm and 31.42 μm respectively.

4. Conclusion

In this work we describe a method for interrogating a spectral interferometer using a scattering medium. Although there are numerous errors associated with the scanning stage kinematics e.g. roll, pitch and flatness which limit the resolution (27 nm) in current system, we have demonstrated that speckle patterns created with a spectral interferometer using a SLED source can be resolved over a range of 500 μm. The scattering spectrometer can successfully extract position information from broadband heavily modulated spectrum. Successful measurements of a 2D profile highlight the method's potential for the use in topography, distance, strain, temperature, pressure measurements and more. Use of a broadband light source has the additional advantage that each measurement point only requires a single measured speckle pattern, compared to the many speckle patterns required for wavelength scanning WLI approaches. This will have an important impact on the measurement rate of such methods all while achieving a drastic reduction in size and cost of spectrometers.

Funding

This work was supported by UK Engineering and Physical Sciences Research Council [grant number EP/P006930/1, EP/N00762X/1], UK Research and Innovation [grant number MR/S034900/1], European Research Council [grant number 804626], Royal Academy of Engineering.

CRediT authorship contribution statement

Qi Sun: Investigation, Validation, Writing – original draft, Visualization. **James Williamson:** Investigation, Resources, Writing – original draft. **Tom Vettenburg:** Data curation, Writing – review & editing. **David B. Phillips:** Conceptualization, Methodology, Writing – review & editing. **Haydn Martin:** Supervision, Writing – review & editing. **Gilberto Brambilla:** Funding acquisition, Resources. **Xiangqian Jiang:**

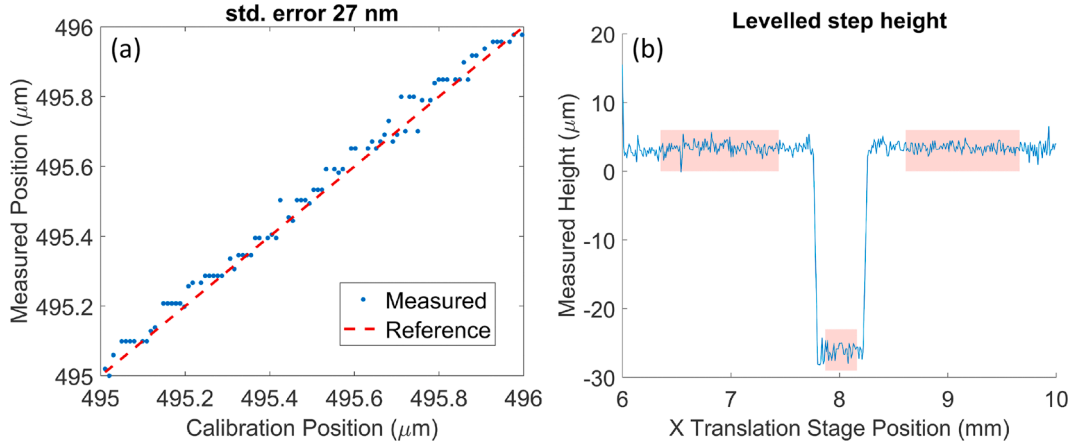

Fig. 4. (a) Resolution test of the scattering chip. The blue marker shows the reconstructed position with speckle pattern of test group. The calibration increment is set to 5 nm over 1 μm range. The red dashed line shows a least-squares linear fit to the data. (b) Measured profile of Rubert 513 step sample. MountainsMap used to apply least squares levelling with exclusion of the step, followed by ISO 5436 step height measurement with automatic detection of negative steps. (For interpretation of the references to colour in this figure legend, the reader is referred to the web version of this article.)

Funding acquisition, Resources. **Martynas Beresna:** Conceptualization, Supervision, Writing – review & editing.

Declaration of Competing Interest

The authors declare that they have no known competing financial interests or personal relationships that could have appeared to influence the work reported in this paper.

Data availability

Data will be made available on request.

References

[1] Redding B, Alam M, Seifert M, Cao H. High-resolution and broadband all-fiber spectrometers. Optica 2014;1(3):175–80.

[2] Mazilu M, Vettenburg T, Di Falco A, Dholakia K. Random super-prism wavelength meter. Opt Lett 2014;39(1):96–9.

[3] Redding B, Liew SF, Sarma R, Cao H. Compact spectrometer based on a disordered photonic chip. Nat Photonics 2013;7(9):746–51.

[4] Wan Y, Wang S, Fan X, Zhang Z, He Z. High-resolution wavemeter using Rayleigh speckle obtained by optical time domain reflectometry. Opt Lett 2020;45(4):799–802.

[5] Facchin M, Dholakia K, Bruce GD. Wavelength sensitivity of the speckle patterns produced by an integrating sphere. J Phys Photonics 2021;3(3):035005.

[6] Sun Q, Vettenburg T, Lee T, Phillips D, Beresna M, Brambilla G. Compact spectrometer chips based on fs laser written multi-layer scattering medium. Asia Communications and photonics conference. Optical Society of America; 2019. p. T4D–5.

[7] Pavlíček P, Häusler G. White-light interferometer with dispersion: an accurate fiber-optic sensor for the measurement of distance. Appl Opt 2005;44(15):2978–83.

[8] Depiereux F, Lehmann P, Pfeifer T, Schmitt R. Fiber-optical sensor with miniaturized probe head and nanometer accuracy based on spatially modulated low-coherence interferogram analysis. Appl Opt 2007;46(17):3425–31.

[9] Williamson J, Martin H, Jiang X. High resolution position measurement from dispersed reference interferometry using template matching. Opt Express 2016;24(9):10103–14.

[10] Huang Y, Wei T, Zhou Z, Zhang Y, Chen G, Xiao H. An extrinsic Fabry–Perot interferometer-based large strain sensor with high resolution. Meas Sci Technol 2010;21(10):105308.

[11] Williamson J, Henning A, Martin H, Furness T, Fletcher S, Jiang X. Flexible gauge length intrinsic fiber-optic strain sensor using broadband interferometry. JOSA A 2020;37(12):1950–7.

[12] Abbas B, Khalil MA. An experimental method for determination of the refractive index of liquid samples using michelson interferometer. Acta Phys Polonica A 2016;129:59.

[13] Arosa Y, Lago EL, Varela LM, de la Fuente R. Spectrally resolved white light interferometry to measure material dispersion over a wide spectral band in a single acquisition. Opt Express 2016;24(15):17303–12.

[14] Wan Y, Fan X, Wang S, Zhang Z, Xu B, He Z. Rayleigh speckle-based wavemeter with high dynamic range and fast reference speckle establishment process assisted by optical frequency combs. Opt Lett 2021;46(6):1241–4.

[15] Bruce GD, O'Donnell L, Chen M, Dholakia K. Overcoming the speckle correlation limit to achieve a fiber wavemeter with attometer resolution. Opt Lett 2019;44(6):1367–70.

[16] Glezer E, Milosavljevic M, Huang L, Finlay R, Her T-H, Callan JP, et al. Three-dimensional optical storage inside transparent materials. Opt Lett 1996;21(24):2023–5.

[17] Falak PL, Sun Q, Vettenburg T, Lee T, Phillips DB, Brambilla G, Beresna M. Femtosecond laser written scattering chip for high-resolution low-cost reconstructive spectrometry. Photonic instrumentation engineering IX. vol. 12008. SPIE; 2022. p. 127–34.